Journal of Materials Chemistry A

Accepted Manuscript

This is an *Accepted Manuscript*, which has been through the Royal Society of Chemistry peer review process and has been accepted for publication.

Accepted Manuscripts are published online shortly after acceptance, before technical editing, formatting and proof reading. Using this free service, authors can make their results available to the community, in citable form, before we publish the edited article. We will replace this *Accepted Manuscript* with the edited and formatted *Advance Article* as soon as it is available.

You can find more information about *Accepted Manuscripts* in the Information for Authors.

Please note that technical editing may introduce minor changes to the text and/or graphics, which may alter content. The journal's standard Terms & Conditions and the Ethical guidelines still apply. In no event shall the Royal Society of Chemistry be held responsible for any errors or omissions in this *Accepted Manuscript* or any consequences arising from the use of any information it contains.

ROYAL SOCIETY OF CHEMISTRY

www.rsc.org/materialsA

Journal Name

RSC Publishing

COMMUNICATION

Three-dimensional MnO_2 Ultrathin Nanosheet Aerogel for High-Performance Li-O_2 Batteries

Cite this: DOI: 10.1039/x0xx00000x

Sheng Chen,[a] Guoxue Liu,[b] Hossein Yadegari,[c] Haihui Wang,[b] and Shi Zhang Qiao[a*]

Received ooth January 2012,
Accepted ooth January 2012

DOI: 10.1039/x0xx00000x

www.rsc.org/

Abstract: Two-dimensional (2D) ultrathin nanocrystals represent a family of emerging nanomaterials with many proposed applications; however, the interlayer re-stacking between sheets greatly decreases the performances during practical operation. This work demonstrates a facile strategy to solve this challenging problem by rational assembly of 2D nanocrystals into three-dimensional (3D) aerogels, which paves the way to harvest excellent structural properties of both nanostructures and macrostructures. The resultant 3D MnO_2 aerogel shows significantly increased discharge capacity in Li-air batteries in comparison to its powder-like counterpart (4581.4 *vs.* 3902.6 mAh g^{-1}), which outperforms many MnO_2 and other transition metal-based electrocatalysts. Meanwhile, the as-fabricated Li-air cell demonstrates good rate capability and cycle life. Further mechanism study reveals that the improved performance is associated with ultrathin MnO_2 nanosheets which allows highly exposed catalytic centres, as well as its excellent aerogel structure with rich porosity and 3D continuous network that maximizes the utilization of MnO_2 species for catalytic reactions. This study may open up new opportunities for making full use of 2D nanocrystals for a number of energy storage/conversion techniques.

Nowadays, two-dimensional (2D) ultrathin nanocrystals, such as molybdenum disulfide (MoS_2),[1, 2] graphitic carbon nitrate (g-C_3N_4),[3] nickel cobaltite ($NiCo_2O_4$),[4] and manganese dioxide (MnO_2),[5] have attracted extensive interest owning to their modified electronic, physical, and electrochemical properties as compared to their bulk counterparts. This new class of materials has been proposed to be used in a number of applications such as catalysis, sensors, absorbents and energy storage/conversion.[1-5] However, owning to their high surface energy and *van deer Waals forces*, 2D ultrathin nanocrystals tend to restack and condense which may compromise their performances during practical applications.[1] To address this obstacle, many strategies have been put forward in the literature such as the addition of "spacers" between nanosheets[6] and layer-by-layer assembly of 2D materials[5]. Most research has been focused on maintaining the integrity of 2D architecture; however, these methods are complicated, and the performances remain unsatisfactory. Recently, there has been great interest in the study of assembling 2D nanocrystals into hierarchical microstructures, for example, integrating MoS_2 nanosheets into hollow tubes[1] and $NiCo_2O_4$ into nanoflowers.[4] These studies provide new clues to inhibit the aggregation of 2D ultrathin nanosheets, and the as-resultant microstructures have been utilized for various applications with enhanced properties. Nevertheless, most reported microstructures are prepared in the form of powders, and the aggregation of these microstructures during post synthesis processes is significant (such as drying in the oven), resulting in reduced accessible surface area and porosity. As a result, it remains great challenge to prohibit the restacking of 2D nanocrystals for achieving optimized electrochemical and/or catalytic properties.

On the other hand, Li-O_2 batteries have received much attention in recent years owning to their higher energy densities than common Li-ions batteries (11,680 *vs.* ~300 Wh kg^{-1}), which make them appealing candidates in the applications such as portable electronics, vehicle transportation, and smart grids.[7, 8] The heart of a Li-O_2 battery is cathode (also named as air electrode), in which the reversible formation and decomposition of lithium peroxide (Li_2O_2) *via* oxygen reduction reaction (ORR) and oxygen evolution reaction (OER) play a key role in the discharge and charge processes.[12, 19] To facilitate the kinetics of ORR/OER, various electrocatalysts have been developed including carbons-based materials, transition metal oxides, noble metals, *etc*.[9-11] Among them, transition metal oxides in particular manganese dioxide (MnO_2) have been widely investigated because of their high intrinsic activity, low cost, abundance, and environmental friendliness.[11, 12] However, bulk MnO_2 only delivers moderate catalytic performance because of the lack of open channels for lithium ions and oxygen gas access and transport. The reduction in particle thickness into atomic level to generate 2D MnO_2 ultrathin nanosheets can significantly increase the accessible surface

Journal of Materials Chemistry A Accepted Manuscript

area, cut ion migration path length, and facilitate reaction kinetics. Nevertheless, 2D MnO_2 nanosheets might tend to aggregate with each other during the operation process, which greatly decrease the discharge capacity of Li-O_2 batteries.

Three-dimensional (3D) macroscopic assemblies, such as aerogels and hydrogels, represent a category of materials that features low densities, large open pores, high inner surface areas, and superior physical and chemical properties.[13-15] Therefore, the assembly of 2D nanocrystals into 3D aerogels/hydrogels might provide a new solution to the challenging problems of nanosheet aggregation. Indeed, our previous works have provided some insight into this hypothesis. We have prepared a number of 3D aerogel/hydrogel catalyst electrodes on the basis of 2D graphene sheets and other nanoparticles ($NiCo_2O_4$,[14] carbon nanotubes,[15]*etc*), which exhibited significantly enhanced OER catalytic properties as compared to their powder-like counterparts. Since OER is a reverse process of ORR, and both of them are critical processes of Li-O_2 batteries; it is expected that the assembly of 2D nanocrystals into 3D aerogels will lead to an improved performance in Li-O_2 batteries. To our best knowledge, the reports of 3D MnO_2 ultrathin nanosheet aerogel for Li-O_2 batteries are rare.

Herein, we report the work of bottom-up assembly of 2D MnO_2nanosheets into 3D aerogels (denoted as 3D MnO_2). The as-resultant material can combine a number of excellent structural properties such as highly exposed active sites, rich porosity, and 3D continuous network, making it a promising catalyst for many electrochemical applications.Li-O_2cells with 3D MnO_2 as catalyst shows significantly increased discharge capacity, which outperforms those of many MnO_2 and other transition metal-based electrocatalysts.

3D MnO_2 was synthesized according to the procedure shown in Scheme 1. In the first step, MnO_2 ultrathin nanosheets were assembled into nanoflowers by chemical reaction of manganese precursors in a water/dimethylformamide (DMF) mixed solution (step A). Subsequently, the as-produced material was dispersed in water, frozen by liquid nitrogen (step B), and thawed in a freeze drier (step C).

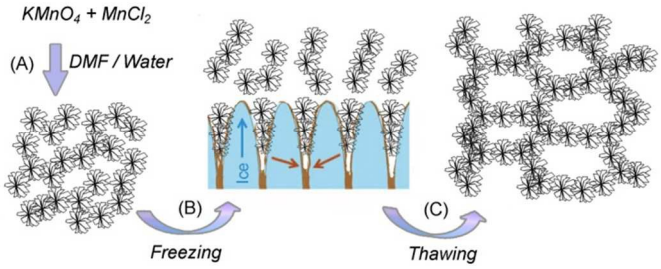

Scheme 1. Synthetic process of 3D MnO_2: (A) Reaction of $KMnO_4$ and $MnCl_2$ in a DMF/water mixed solvent to assemble MnO_2 ultrathin nanosheets into nanoflowers; (B) freezing in liquid nitrogen; (C) thawing in a freeze drier.

The optical image in Figure 1A reveals that 3D MnO_2 has a self-supported macroscopic cylinder structure around 0.8 cm in diameter and several centimetres in length. The material has a well-developed 3D continuous network with the pore size ranging from several to tens of micrometers (Figure 1B). The techniques such as element mapping (Figure 1C), transmission electron microscopy (TEM, Figure 1D,E) and atomic force microscopy (AFM, Figure S1) confirm the flower-like morphology of MnO_2 around 200 nm size constructed with intersected ultrathin nanosheets. The ultrathin MnO_2nanosheets tend to curl and fold, thus providing an opportunity to directly measure their thickness from the vertical edges. High resolution transmission electron microscopy (HRTEM, Figure 1F) reveals the typical thickness of nanosheets is around 3.6 nm, corresponding to 3~4 layered MnO_2 crystal unit cells.[5]

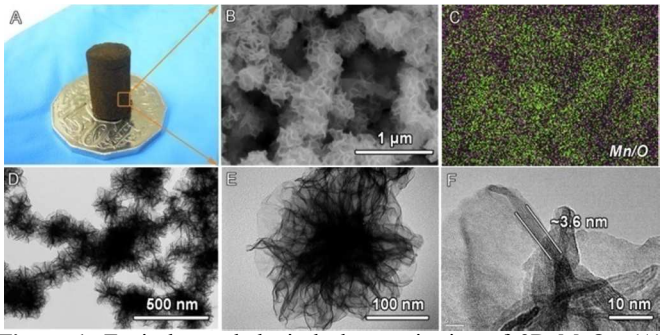

Figure 1. Typical morphological characterization of 3D MnO_2: (A) optical image; (B) SEM image; (C) EDS element mapping taken from the area in panel (B) showing distribution of Mn and O atoms; (D,E)TEM images; (F) HRTEM image.

XRD pattern (Figure 2A) of 3D MnO_2 reveals four prominent peaks that match well with δ-MnO_2 (JPCDS card no. 80-1098). As compared to its powder-like counterpart prepared without freezing-dry (see experimental section), 3D MnO_2 aerogel shows a significantly weakened diffraction peaks, indicating that single MnO_2nanosheet in the 3D structure are largely separated. Moreover, nitrogen adsorption isotherm shown in Figure 2B resembles type IV with a narrow hysteresis loop. The corresponding pore size distribution obtained by BJH method shows the presence of both mesopores and small macropores ranging from 15 to 60 nm (inset in Figure 2B).[16] The Brunauer, Emmett and Teller (BET) surface area of 3D MnO_2 is as higher as 156 m^2 g^{-1}, and its pore volume is 0.56 cm^3 g^{-1}. The relatively high surface area with rich porosity may provide more accessible surface for catalytic processes.

The chemical structure of 3D MnO_2 was detected using X-ray photoelectron spectroscopy (XPS, Figure 2C); the peaks of Mn 2p3/2 and 2p1/2 are centred at 657.1 and 654.3 eV, respectively, with a spin energy separation of 11.8 eV in agreement with reported data of Mn 2p3/2 and Mn 2p1/2 in MnO_2. Energy-dispersive X-ray spectroscopy (EDS) further verifies the formation of MnO_2 material, where only Mn, O, C, and Pt can be observed (C emanates from carbon coated SEM tap, and Pt from Pt coatings, Figure 2D). The Raman spectrum of MnO_2 is characterized by two sharp peaks at 457 and 635 cm^{-1} along with four weak bands at 216, 354, 554 and 753 cm^{-1} (Figure 2E). The main contributions of these peaks are stretching mode of MnO_6octahedra in MnO_2.[17] Moreover, thermogravimetric analysis (TGA, Figure 2F) plot of 3D MnO_2 indicates a continuous weight loss from 120 to 500 ^oC

Journal of Materials Chemistry A Accepted Manuscript

This journal is © The Royal Society of Chemistry 2012

originating from the removal of physisorbed water (~120 °C), structural water (~200 °C) and phase transition from MnO_2 to Mn_2O_3 (~500 °C).

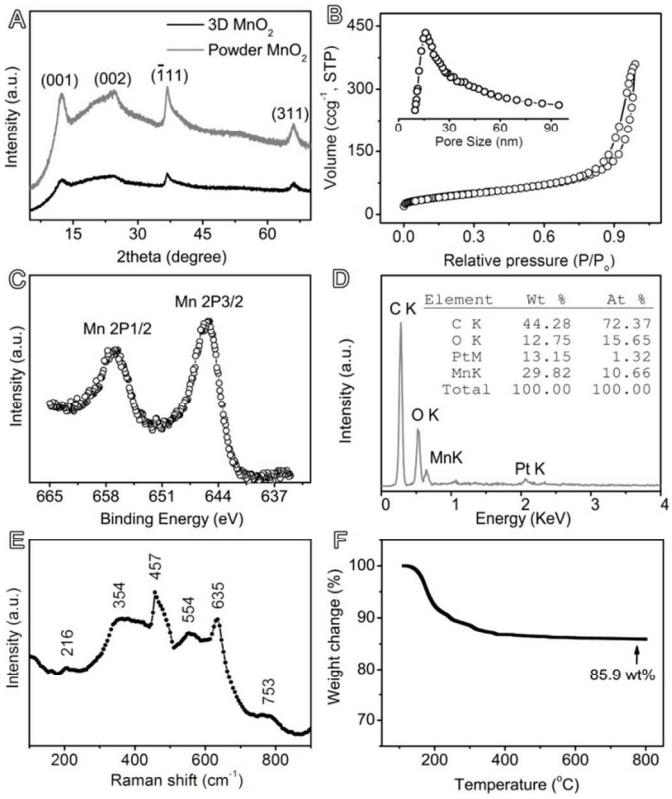

Figure 2. The structural analyses of 3D MnO_2: (A) XRD as compared to that of powder MnO_2; (B) nitrogen adsorption-desorption isotherm (expressed in cm^3 STP g^{-1}); the inset shows the corresponding pore size distribution (expressed in cm^3 g^{-1} nm^{-1}); (C) XPS Mn2p spectrum; (D) Element analysis; (E) Raman spectrum (unit of peak positions: cm^{-1}); (F) TGA plot.

The formation mechanisms of 3D MnO_2 are studied on the basis of a series of controlled experiments. There are two steps in the preparation processes, *i.e.*, assembly of MnO_2 ultrathin nanosheets into nanoflowers and subsequent freeze-drying into 3D aerogel. In the first step, time-dependent experiments from 1 to 30 min are conducted to examine the intermediate crystal growth products of MnO_2 nanoflower. The analyses of zeta-potential (Figure 3A), TEM (Figure S2), and UV-vis spectra (Figure S3) suggest that dissolution-crystallization mechanism is responsible for this process where less ordered MnO_2 precursors gradually disappear with the emergence of more nanoflowers.[6] Of particular interest is that DMF plays a key role in the formation of MnO_2nanoflowers. FT-IR spectrum of MnO_2 shows -CH_3 stretching vibrations at 2800−3000 cm^{-1} and C=O modes at 1700 cm^{-1} (Figure 3B), which indicate that the surface of MnO_2 are capped with DMF (chemical structure: $(CH_3)_2NC(O)H$)). Moreover, a high DMF/water ratio (from 0/55 to 10/45, 20/35 and 40/15) is beneficial to the formation of MnO_2nanoflowers (Figure S4), thus indicating DMF serves both as a solvent and a surface ligand during crystal growth.[1]

In the second step, MnO_2nanoflowers are frozen in a liquid nitrogen bath. In this process, phase separation between water and ice can result in the rejection of solid nanoparticles, where MnO_2 is entrapped between neighboring ice crystals (Scheme 1).[18] Because the growth rate of ice crystals is highly anisotropic, MnO_2nanoflowers are forced to align and concentrated along the moving solidification front to form a continuous 3D network. Subsequent sublimation of ice leads to the formation of MnO_2 aerogel. The interactions between MnO_2nanoflowers in 3D architecture is proposed as *van der Waals*' forces and hydrogen bondings as indicated by the presence of C-O and –OH groups in MnO_2dispersion (Figure 3B).

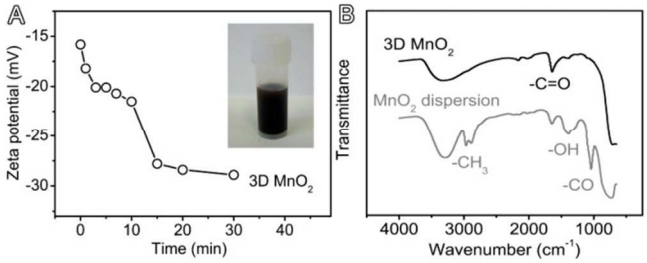

Figure 3.(A) Zeta potential of MnO_2 dispersions taken directly from reaction solution at different intervals; the inset shows an optical image of MnO_2 dispersion; (B) FTIR spectra of 3D MnO_2 and MnO_2 dispersion.

The as-prepared 3D MnO_2 aerogel was mixed with Ketjenblack carbon and polyvinylidene fluoride (PVDF) in molar ratio 30:60:10, and fabricated into catalyst electrodes for Li-O_2 batteries. For comparison, its counterpart without 3D architecture (*i.e.* "powder MnO_2") was also evaluated under the similar condition. The Li-O_2 cells exhibited a discharge voltage around 2.85 V *vs.* Li^+/Li^0, which is higher than that of the powder MnO_2 by 60-80 mV, and corresponding to the transition from Li^+ into Li_2O_2*via* ORR process (Figures 4A).[13, 22] The charge voltage of the Li-O_2 cells with 3D MnO_2 was much lower than that of the powder MnO_2 by around 130 mV, corresponding to the transition from Li_2O_2 into Li^+ *via* OER process. Note that 3D MnO_2 aerogel is more effective for catalyzing OER and ORR as compared to powder MnO_2, indicating the unique aerogel structure plays an important role during discharge and charge processes of Li-O_2 batteries. To our best knowledge, the discharge capacity of 3D MnO_2 (4581 mAh g^{-1}) outperforms those of many transition metal-based electrocatalysts reported in the literature (Table S1), such as Fe_2O_3 (2700 mAh g^{-1})[19], α-MnO_2 nanowires (3000 mAh g^{-1})[11], and MnO_2-carbon nanotubes composite (2247 mAh g^{-1})[20].

Besides discharge capacity, Li-O_2 cells with 3D MnO_2 also shows good rate capability (Figure 4B). The initial discharge capacity is 4581mAh g^{-1} at 50 mA g^{-1}. The discharge capacities only gradually decrease at higher current densities, which are 2727 mAh g^{-1}at 100 mA g^{-1}, 2343 mAh g^{-1} at 200 mA g^{-1}, and 1519 mAh g^{-1} at 300 mA g^{-1}, respectively. This phenomenon might be explained by the rich porosity and 3D continuous network of 3D MnO_2 aerogel, which can increase the utilization of active species at high current densities, and provide more access to the capacities. Further, cycling performances of Li-O_2 cell with 3D MnO_2 are shown in Figures 4C,D. The Li-O_2 cells with 3D MnO_2 was cycled at a 1000 mAh g^{-1} capacity limit for 25 cycles with stable discharge-charge voltage platforms, demonstrating good electrode stability.[7, 21, 22]

Journal of Materials Chemistry A Accepted Manuscript

The observed performance enhancement in 3D MnO_2 indicates that the proposed electrocatalyst is favourable for energy storage in Li-O_2 batteries. Firstly, the ultrathin nanosheets in 3D MnO_2 afford highly accessible catalytic centres to facilitate the ORR/OER processes.[1, 2] The reduction in particle thickness has led to a much higher discharge capacity in 3D MnO_2 than its powder counterpart (4581.4 *vs.* 3902.6 mAh g^{-1}, Figure 4A). On the other hand, the formation of 3D macroscopic aerogel by the freeze-dryer method can effectively inhibit the restacking in MnO_2 ultrathin nanosheets, thus enabling the maximal use of active centres for catalytic reactions. The formation of well-defined macro/mesoporosity is confirmed by both nitrogen adsorption and XRD analysis (Figure 2A,B). These porous structure can reduce the migration path length of both oxygen molecules and lithium ions,[23, 24] thereby significantly enhancing the rate capability in Li-O_2 cells. Further, the excellent stability can be explained by the rich 3D hierarchical porous structure that can accommodate the as-formed Li_2O_2 during the discharging-charging process.[11]

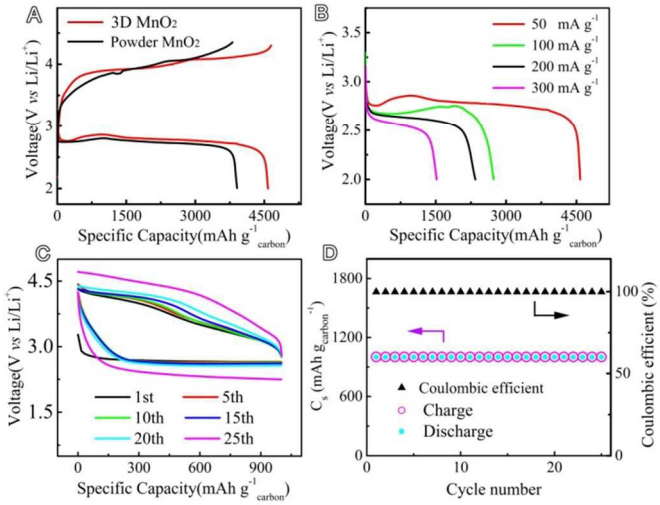

Figure 4. (A) Discharge plots of Li-O_2 battery cells with 3D MnO_2 and powder MnO_2 catalysts at 50 mA g^{-1}; (B) discharge plots with 3D MnO_2 at different current densities; (C,D) Cycle performances with 3D MnO_2 at 300 mA g^{-1}

The recent researches of Li-O_2 battery mainly focus on mechanism studies of electrochemical process and Li storage and transport.[7, 25] On the other hand, electrode materials are also critical elements of Li-O_2 battery which are directly associated with the efficiency, kinetics and stability of battery.[26, 27] The aim of this work is to design new architectured cathodes for Li-O_2 battery. We have introduced an emerging category of nano-materials as cathodes, *i.e.*, 2D ultrathin nanocrystals, which can provide enormous active centres for enhanced ORR and OER catalytic activities during discharging and charging processes. In view of their tendency to aggregation, 2D ultrathin nanocrystals have been assembled into 3D aerogels for practical applications. To our best knowledge, despite of a few previous reports regarding MnO_2 nanoflowers,[28, 29] the study of 3D MnO_2 ultrathin nanosheet aerogel for Li-O_2 battery has been scarcely reported.

In conclusion, this work reports the first bottom-up synthesis of MnO_2 ultrathin nanosheet aerogels for Li-O_2 batteries. The new material is greatly favorable for ORR/OER, and shows a higher discharge capacity than its counterparts without 3D architecture. Meanwhile, Li-O_2 cell with 3D MnO_2 demonstrates good rate capability and cycling performance. Further study reveals that the dissolution-crystallization and ice-assisted freeze-drying processes play a critical role in the rational assembly of 2D nanosheets. The catalyst is synthesized through a facile solution strategy, which can be easily extended to the preparation of many other nanomaterials for a broad range of applications in catalysis, solar cells and energy conversion.

This work is financially supported by the Australian Research Council (ARC) through the Discovery Project programs (DP140104062 and DP130104459).

Notes and references

[a]School of Chemical Engineering, The University of Adelaide, Adelaide, SA 5005, Australia. Fax: +61 8 8303 4373; Tel: +61 8 8313 6443; E-mail: s.qiao@adelaide.edu.au
[b]School of Chemistry & Chemical Engineering, South China University of Technology, No. 381 Wushan Road, Guangzhou 510640, China
[c]Department of Mechanical and Materials Engineering, University of Western Ontario, 1151 Richmond Street N., London, Ontario, Canada N6A 5B9

Electronic Supplementary Information (ESI) available: [Synthetic procedure; AFM analysis of MnO_2nanoflowers; TEM images and UV-vis spectra of MnO_2 dispersions taken directly from reaction solution at different time intervals; TEM images of MnO_2 dispersions prepared with different water/DMF ratios; charge profiles of 3D MnO_2 aerogel and power MnO_2; Charge-discharge plots of Li-O_2batterieswith 3D MnO_2 at different current densities; a table for comparison of Li-O_2battery performance of 3D $MnO_2$with some representative transition metal oxide/hydroxide nanostructures recently reported in the literature]. See DOI:10.1039/c000000x/

1. P. P. Wang, H. Sun, Y. Ji, W. Li and X. Wang, *Adv. Mater.*, 2014, **26**, 964-969.
2. J. Xie, H. Zhang, S. Li, R. Wang, X. Sun, M. Zhou, J. Zhou, X. W. Lou and Y. Xie, *Adv. Mater.*, 2013, **25**, 5807-5813.
3. X. Zhang, X. Xie, H. Wang, J. Zhang, B. Pan and Y. Xie, *J. Am. Chem. Soc.*, 2013, **135**, 18-21.
4. C. Yuan, J. Li, L. Hou, X. Zhang, L. Shen and X. W. D. Lou, *Adv. Funct. Mater.*, 2012, **22**, 4592-4597.
5. L. Peng, X. Peng, B. Liu, C. Wu, Y. Xie and G. Yu, *Nano Lett.*, 2013, **13**, 2151-2157.
6. S. Chen, J. Zhu, X. Wu, Q. Han and X. Wang, *ACS Nano*, 2010, **4**, 2822-2830.
7. Z. Peng, S. A. Freunberger, Y. Chen and P. G. Bruce, *Science*, 2012, **337**, 563-566.
8. P. G. Bruce, S. A. Freunberger, L. J. Hardwick and J. M. Tarascon, *Nat. Mater.*, 2012, **11**, 19-29.
9. J. Xiao, D. Mei, X. Li, W. Xu, D. Wang, G. L. Graff, W. D. Bennett, Z. Nie, L. V. Saraf, I. A. Aksay, J. Liu and J. G. Zhang, *Nano Lett.*, 2011, **11**, 5071-5078.
10. Y.-C. Lu, Z. Xu, H. A. Gasteiger, S. Chen, K. Hamad-Schifferli and Y. Shao-Horn, *J. Am. Chem. Soc.*, 2010, **132**, 12170-12171.
11. A. Debart, A. J. Paterson, J. Bao and P. G. Bruce, *Angew. Chem. Int. Ed.*, 2008, **47**, 4521-4524.
12. L. Trahey, N. K. Karan, M. K. Y. Chan, J. Lu, Y. Ren, J. Greeley, M. Balasubramanian, A. K. Burrell, L. A. Curtiss and M. M. Thackeray, *Adv. Energy Mater.*, 2013, **3**, 75-84.
13. Z. Y. Wu, C. Li, H. W. Liang, J. F. Chen and S. H. Yu, *Angew. Chem. Int. Ed.*, 2013, **52**, 2925-2929.
14. S. Chen, J. Duan, M. Jaroniec and S. Z. Qiao, *Angew. Chem. Int. Ed.*, 2013, **52**, 13567-13570.

Journal of Materials Chemistry A Accepted Manuscript

This journal is © The Royal Society of Chemistry 2012

15. S. Chen, J. Duan, M. Jaroniec and S. Z. Qiao, *Adv. Mater.*, 2014, **26**, 2925-2930.
16. M. Kruk, M. Jaroniec and A. Sayari, *Langmuir*, 1997, **13**, 6267-6273.
17. C. Julien, M. Massot, S. Rangan, M. Lemal and D. Guyomard, *J. Raman Spectrosc.*, 2002, **33**, 223-228.
18. S. Deville, E. Saiz, R. K. Nalla and A. P. Tomsia, *Science*, 2006, **311**, 515-518.
19. A. Débart, J. Bao, G. Armstrong and P. G. Bruce, *J. Power Sources*, 2007, **174**, 1177-1182.
20. J. Li, N. Wang, Y. Zhao, Y. Ding and L. Guan, *Electrochem. Commun.*, 2011, **13**, 698-700.
21. J. Wang, Y. Li and X. Sun, *Nano Energ.*, 2013, **2**, 443-467.
22. S. H. Oh, R. Black, E. Pomerantseva, J.-H. Lee and L. F. Nazar, *Nat. Chem.*, 2012, **4**, 1004-1010.
23. Y. Li, X. Li, D. Geng, Y. Tang, R. Li, J.-P. Dodelet, M. Lefèvre and X. Sun, *Carbon*, 2013, **64**, 170-177.
24. F. Cheng and J. Chen, *Nat. Chem.*, 2012, **4**, 962-963.
25. L. Johnson, C. Li, Z. Liu, Y. Chen, S. A. Freunberger, P. C. Ashok, B. B. Praveen, K. Dholakia, J. M. Tarascon and P. G. Bruce, *Nat. Chem.*, 2014, **6**, 1091-1099.
26. F. Li, Y. Chen, D.-M. Tang, Z. Jian, C. Liu, D. Golberg, A. Yamada and H. Zhou, *Energy Environ. Sci.*, 2014, **7**, 1648.
27. E. Yoo, J. Nakamura and H. Zhou, *Energy Environ. Sci.*, 2012, **5**, 6928.
28. S. Liu, Y. Zhu, J. Xie, Y. Huo, H. Y. Yang, T. Zhu, G. Cao, X. Zhao and S. Zhang, *Adv. Energy Mater.*, 2014, **4**, DOI: 10.1002/aenm.201301960.
29. D. Li, G. Du, J. Wang, Z. Guo, Z. Chen and H. Liu, *J. Chin. Chem. Soc.*, 2012, **59**, 1211-1215.

Journal of Materials Chemistry A Accepted Manuscript